AD-A043 591 WASHINGTON UNIV ST LOUIS MO LAB FOR APPLIED ELECTRON--ETC F/G 20/6
TIME AND FREQUENCY DEMULTIPLEXING IOC RECEIVERS.(U)
APR 76 W S CHANG, C M WOLFE
N00014-75-C-1155 NL

UNCLASSIFIED

1 OF 1
AD A043591

END
DATE FILMED
9-77
DDC

(8)
D.S.

(2)

TIME AND FREQUENCY DEMULTIPLEXING IOC RECEIVERS.

(11) 29 Apr 76

By

(10) W. S. C. Chang and C. M. Wolfe
Department of Electrical Engineering
and
Laboratory for Applied Electronic Sciences
Washington University
St. Louis, Missouri 63130

(12) 23 p.

(9) Progress Report, 1 Jul 75 - 20 Apr 76.
April 29, 1976

Prepared Under
Contract No. (15) N00014-75-C-1155
For
Dr. David C. Lewis
Office of Naval Research (Code 221)
800 N. Quincy Street
Arlington, Virginia 22217

408607

SUMMARY

During the period from 1 July, 1975 to 20 April, 1976, the following progress has been made toward the realization of an IOC receiver. ~~under this contract:~~

(1) GaAs electroabsorption avalanche photodiode (EAP) detectors with responsivities up to 60 A/W have been successfully fabricated in single-mode waveguide structures and evaluated experimentally.

(2) The effects of doping, applied voltage, and device dimensions on the performance of EAP waveguide detectors has been evaluated theoretically as an aid to device and system optimization.

(3) Using this analysis a three-channel frequency demultiplexing receiver using EAP waveguide detectors has been designed.

(4) A three-channel, 1 M bit/sec time demultiplexing system has been designed, constructed, and demonstrated.

1. WAVEGUIDE DETECTORS

1.1 Design and Fabrication of GaAs EAP Detectors

The design considerations in the original proposal indicated that the discrete GaAs electroabsorption avalanche photodiode (EAP), originally developed by Stillman and Wolfe[1] could be incorporated into a single-mode waveguide for use as an integrated optical circuit (IOC) receiver. If the waveguide were fabricated from high-purity GaAs grown epitaxially on a GaAs substrate doped at 1×10^{18} cm^{-3}, the heavy doping of the substrate would suppress the index of refraction enough to support a single mode in a waveguide thickness of about 6 μm. The heavily-doped substrate would also serve as a closely-spaced back contact to obtain a low impedance device. The high-purity epitaxial GaAs would transmit GaAs laser wavelengths greater than 0.905 μm with losses less than 1 cm^{-1}[2] and also provide a guard-ring[3] for the EAP detector. Since response speed measurements on discrete devices indicated rise times of less than 1 nsec[1] the EAP waveguide detectors should be useful for high-data-rate optical communication. This initial analysis also indicated that the internal quantum efficiency (without gain) of the waveguide device should depend on its length with values from 80 to 100 percent obtainable for GaAs laser wavelengths using device lengths of 100 μm. Avalanche gain, however, should depend on the thickness of the depletion region and a 6 μm single-mode waveguide would limit the gain to a maximum of about 200, somewhat lower than that achievable in a discrete device. Preliminary analysis also

indicated that the GaAs EAP waveguide detector could be useful for the detection of 1.06 μm.

With these initial design criteria GaAs EAP waveguide detectors were fabricated using the process steps indicated in the proposal. Experience obtained with this procedure, however, dictated a number of improvements, and the revised process is outlined in Fig. 1. To obtain the detector material, a 10-μm thick layer doped with Sn at 5×10^{15} cm^{-3} is grown epitaxially on an n^+GaAs substrate. Over this epitaxial layer a pyrolytic SiO_2, 3000Å thick, is deposited and patterned photolithographically to leave 5 mil diameter disks of SiO_2 [Fig. 1(a)]. These disks serve as an etch mask, and the epitaxial material around the device regions is then etched away to obtain the structure shown in Fig. 1(b). This structure is then placed in the epitaxial reactor, where the disks now act as a mask against growth. In the reactor, a high-purity layer for the waveguide-guard ring is grown around the device regions [Fig. 1(c)].

After the samples are removed from the reactor, the SiO_2 disks are removed, and, because of the growth morphology, the epitaxially-grown waveguide is polished to a final thickness of 5 - 7 μm. A pyrolytic SiO_2 is now deposited over the surface and a layer of Au-Sn eutectic is electroplated over the back of the n^+ substrate to obtain the structure shown in Fig. 1(d). This Au-Sn layer is alloyed into the material at a temperature of 540°C in a reducing atmosphere to obtain an ohmic contact. Following this step, 5-mil diameter holes with 2-mil diameter

holes for the bonding pads are opened photolithographically in the SiO_2 on the upper surface. In the last step, Au for the Schottky barrier and bonding pads is electroplated in the holes to obtain the structure shown in Fig. 1(e). This appears to be close to an optimum process for fabricating the EAP waveguide detectors.

1.2 Materials and Process Evaluation

During each epitaxial growth process in the devices, a layer is simultaneously grown on a high-resistivity control sample to determine carrier concentration and mobility. In this manner, samples which will not provide the appropriate device structure can be eliminated without additional processing. Material for the device regions is typically doped at 5×10^{15} cm^{-3} with room temperature mobilities of 6000 cm^2/sec, while the undoped high-purity material for the waveguides usually has a carrier concentration of 1×10^{14} cm^{-3} with a mobility of 8000 $cm^2/Vsec$. These values are expected to give close to optimum device performance.

The whole process is evaluated by examining the properties of the finished devices. By isolating regions of the back Au-Sn contact and examining the I-V characteristics between these regions, the back contact was found to be ohmic with a resistance of about 10 ohms. The Au Schottky barriers have a normal 0.5 volt breakdown in the forward direction with the best having an incremented forward resistance of 1 to 2 ohms. In the reverse direction the Schottky barriers have breakdown voltages

(30 to 50 volts) which depend on the doping level and device thickness. The dark current at breakdown is typically less than 1 μamp. The devices appear to be well guarded and can withstand reverse currents in excess of 10 ma without catastropic failure. The resistance beyond breakdown for the best devices has been in the range from 100 to 400 ohms. Many of the devices, however, have reverse resistances in the range from 1000 to 3000 ohms and this is probably limiting the gain in these devices. This high reverse resistance is apparently due to an undoped high resistance region at the substrate-eptaxial layer which is produced by certain types of GaAs substrates. Although (as discussed below) when this type of region is completely depleted of carriers, it can improve device perfromance by giving higher gain at lower fields, when it is undepleted it can lower the maximum gain. The problem can, however, be overcome by either completely depleting the region or using different substrates.

1.3 Theroetical Waveguide Detector Response

To obtain a quantitative understanding of the EAP waveguide detector response, the detector structure, shown in Fig. 1, can be approximated by the structure shown in Fig. 2. The analysis begins by first determining the guided wave modes for a GaAs $n\text{-}n^+$ waveguide, from which we obtain the photon flex density incident on the detector, $\phi_i(x,0)$, for various waveguide thicknesses, W, and doping concentrations. When a reverse bias voltage is applied to the Schottky barrier, the electric field in the depletion region ($t \leq W$) increases and, assuming a uniform

doping profile, the electric field will vary linearly as a function of x until the electric field at x = 0 is equal to the breakdown field. This and other electric field distributions are determined from Poisson's equation. Knowing the electric field distribution and the field dependence of the ionization coefficients[4], the absorption coefficient, α, and the ionization coefficients (α_n for electron and β_p) are calculated as functions of x in the depletion layer and the applied voltage.

The net effect of the absorption coefficient is to cause the photon density to be attenuated as a function of z, i.e.,

$$\phi_i(x,z) = \phi_i(x,0)\ e^{-\Gamma_i z}$$

Using a perturbation approach, Γ_i is calcualted from the ratio of the total power absorbed from each mode within a distance dz to the total energy stored in that mode [i.e., $\hbar\omega\int_0^\infty \phi_i(x,z)\,dx$]. Figure 3 shows the calculated values of Γ_i as a function of applied bias voltage for W = 10 μm, D = 100 μm, N = 5 x 10^{15} cm^{-3} and λ = 0.905 μm. .

We then assume that each absorbed photon produces an electron-hole pair and that these pairs produce secondary pairs by impact ionization. The solutions for the differential equations governing the resulting electron and hole current densities are obtained numerically on a computer. From the calculated photocurrent density, the responsivity, R (the ratio of the photocurrent collected to the amount of power contained in the guided wave mode) has been obtained for various doping concentrations, waveguide

thicknesses, wavelengths, and detector dimensions. Figure 4 shows the responsivity for a typical sample as a function of bias voltage with D = 100 μm, W = 10 μm , $N = 5 \times 10^{15}$ for different wavelengths, λ.

These calculated results are useful for several reasons: (1) they give us design guidelines for the fabrication of experimental devices. For example, these results indicate that to have a detector with good responsitivity at λ = 1.06 μm, we need D ≅ 2 or 3 mm. (2) They enable us to interpret the measured data. For example, a comparison between the values of Γ and R (and their comparison to the measured values) enable us to differentiate between the optical absorption and the electron and hole multiplication processes of the detectors. (3) They give us the necessary initial data upon which a design of a frequency demultiplexing scheme can be made, as will be discussed in Section 3. (4) In contrast to conventional discrete photodetectors, these results show that waveguide detectors should have a flat frequency response for optical energies above the fundamental absorption edge. This is an advantage for those applications in which one wants to have a detector with uniform responsivity at shorter wavelengths.

1.4 Experimental Waveguide Detector Response

We have used two experimental procedures to evaluate the detector response. In the first procedure, either a laser source or a broadband source in conjunction with a Perkin Elmer Model El grating monochromator is used to illuminate the diode detector in a direction normal to the waveguide surface. In the second procedure, a GaAs diode laser is used to directly excite a

a guided wave in the epitaxial waveguide. The energy in the guided wave mode is then detected by the EAP detector. Although the first approach is an indirect evaluation of the waveguide detector, it offers a convenient way in which the electroabsorption effect at different wavelengths can be evaluated directly without a tunable laser source. This first approach has two disadvantages: (1) it requires a transparent electrode, and (2) the coupling efficiency of any incoherent source to the waveguide is too low to permit the evaluation of the detector as a guided wave detector. The second approach directly evaluates the behavior of the device as a waveguide detector. However, the response of the detector at different wavelengths can only be evaluated whenever a laser source is available. So far, most of our data has been obtained using the second approach. The first approach is expected to be used more in the experimental evaluation of the frequency demultiplexing schemes.

The dashed curve in Fig. 3 shows the measured power attenuation coefficient, Γ, of the guided wave mode at 0.905 μm as a function of the applied voltage for a typical detector.* Notice that the measured and calculated values of Γ exhibit about the same variation with applied voltage. The measured values of Γ, however, are larger than the calculated values, indicating that the absorption of the guided wave is stronger than that predicted by theory. We believe that this measured behavior of Γ is caused by the

*The measured Γ value is the average Γ of all of the propagating modes of the waveguide.

doping profile discussed in Section 1.2, and we intend to investigate the effects of the doping profile in more detail.

The dashed curve in Fig. 4 shows the measured responsivity (in A/W) of the detector. Notice that the measured responsivity of this detector is quite good. When compared to the theoretically predicted responsivity, we notice that the measured responsivity is much better than the theoretically-predicted responsivity. This difference could again be caused by the doping profile created during the growth of the epitaxial layer, producing a higher average electric field in the depletion region, thereby increasing both the absorption and the ionization coefficients at relatively low voltage levels. For an avalanche detector, this effect gives an added advantage in that gain fluctuations caused by the voltage fluctuations can be reduced. Various experimental measurements have been planned for the remainder of this contract period to examine and to control this behavior.

2. FREQUENCY DEMULTIPLEXING

From Fig. 3 we see that the amount of the power absorbed by a given detector at a given wavelength depend on the bias voltage. When there are three guided waves at different wavelengths (representing signals from three separate channels) propagating thorugh a series of three detectors biased at different voltages in an increasing order, most of the energy of the guided at the shortest wavelength (i.e., the first channel) will be detected by the first detector. A small amount of that energy will be leaked to the second detector, constituting the cross-talk of the signals in the first channel to the second detector. Conversely, some of the energy at the longer wavelengths will be detected by the first detector, constituting the cross-talk of the longer wavelength channels to the first detector. Similar situations occur at the second and the third detector. We have calculated the cross-talk of the different channels at different wavelengths based upon the numerically calculated values of Γ as a function of bias voltage and wavelength. We have also varied (1) the wavelengths of the guided waves in the three channels, (2) the length of the detector D, and (3) the applied voltage to the three detectors to obtain a design which would minimize cross-talk ratios between channels. Table I shows such a design. Notice that the cross-talk ratio of 10 dB is typically what can be obtained based solely upon the wavelength dependence of the electroabsorption. Much higher isolation between channels can be obtained if only two-wavelength channels are employed.

Due to differences between theory and experiment, the design given in Table I may not be optimum. However, we expect it to represent roughly what can be achieved by such a system. We have thus ordered laser diodes at these wavelengths to experimentally evaluate this scheme.

3. TIME DEMULTIPLEXING

Two time demultiplexing schemes were proposed for the contract. So far we have completed the design and the construction of time demultiplexing circuits where the demultiplexing is carried out by the detector. The design and the construction of electronic circuit for time demultiplexing by the sequential switching of the bias voltages of the detectors is still in the process of being carried out.

Figures 5 and 6 show the schematic diagram of the completed electronic demultiplexing scheme. In this scheme, we have designed an electronic circuit that will generate diode laser (or LED) pulse train consisting of a synchronizing pulse 20 nsec wide, followed by a sequence of three sets of signal pulses. There are 12 pulses 5 nsec wide in each signal pulse set, constituting 12 bits of information in a given channel. After the optical signal is detected by the detector, the pulse width discriminator picks out the synchronizing pulse and activates a sequence of switches that will send the first set of signal pulses to channel A, the second set to channel B, and the third set to channel C. This sequence will repeat after receiving a subsequent synchronizing pulse. This receiver system is fully functional at a 1 Megabit/sec data rate with LED and a T1XL57 avalanche detector. It has also functioned for a laser diode with the EAP waveguide detector at a reduced data rate because of the duty cycle limitations of our present laser diode. We are expecting the deliver of new high-duty-cycle laser diodes.

Thus the 3-channel, 12-bit, 1-Megabit/sec time demultiplexing system should be fully functional within two weeks. However, the bandwidth limitation of the receiver system and the pulse generators for the laser diode are capable of handling 50 Megabits per second data; only the power amplifier of the laser diode driver unit is limiting us to the data rate of 1 Megabits/sec. Thus a new power amplifier is currently being designed to increase the data rate.

REFERENCES

1. G. E. Stillman, C. M. Wolfe, J. A. Rossi, and J. P. Donnelly, Applied Physics Letters 25, p. 671 (1974).

2. G. E. Stillman, C. M. Wolfe, J. A. Rossi, and H. Heckscher, Applied Physics Letters 28, p. 197 (1976).

3. C. M. Wolfe and W. T. Lindley, J. Electrochem Soc. 116, p. 276 (1969).

4. G. E. Stillman, C. M. Wolfe, J. A. Rossi, and J. L. Ryan, Proc. 5th Int. Symp. GaAs (Inst. Physics, London, 1975) p. 210.

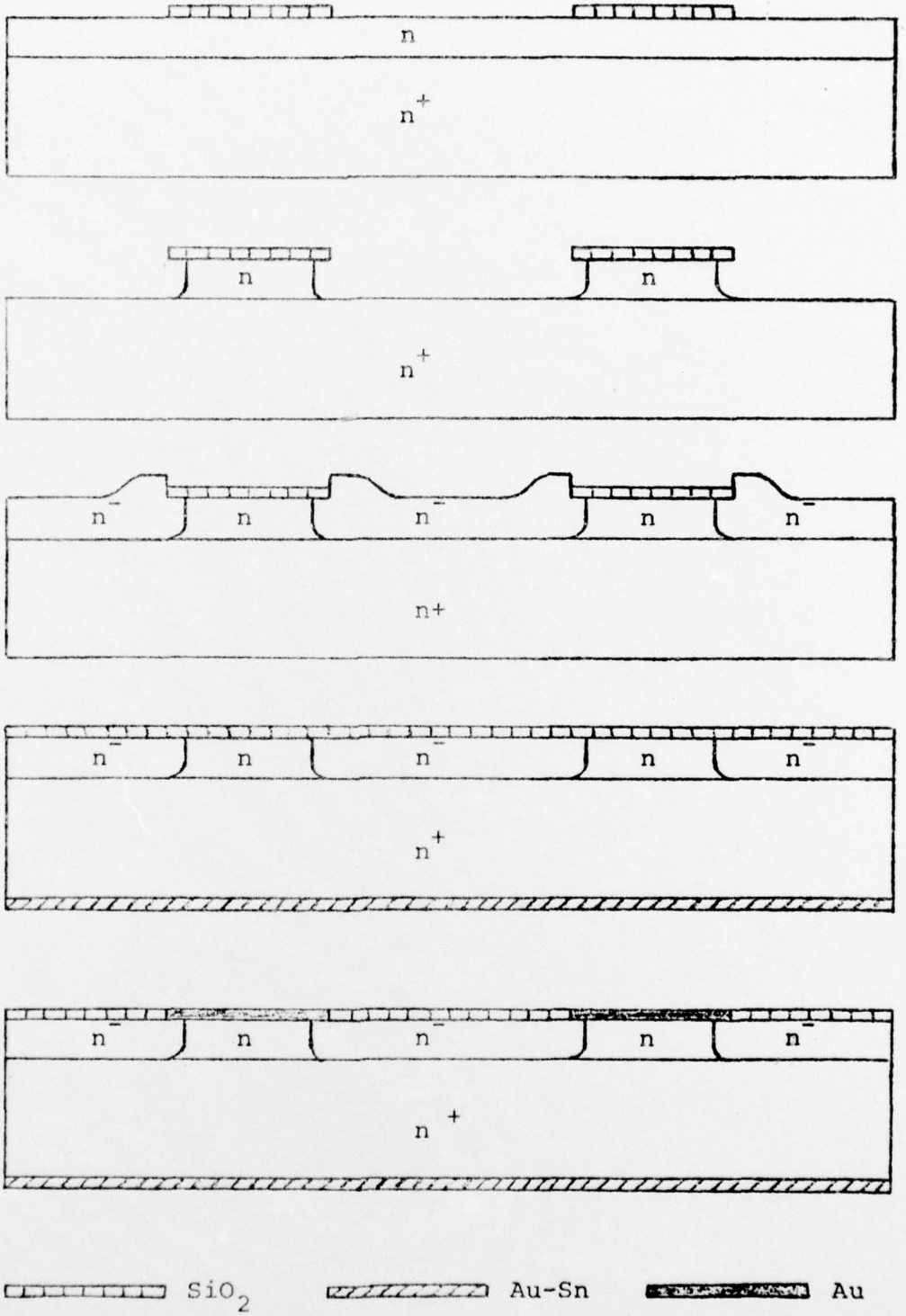

Fig. 1 Fabrication of EAP Waveguide Detectors

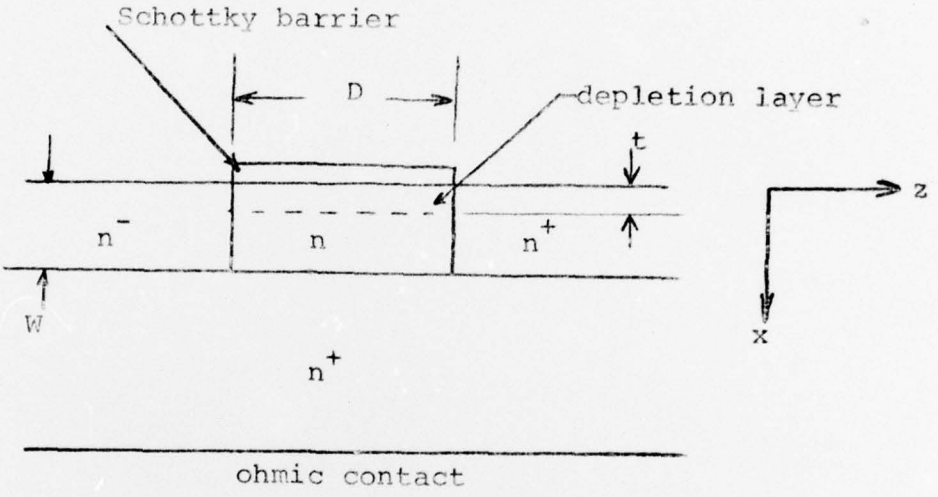

Fig. 2 The Idealized Structure for Analysis

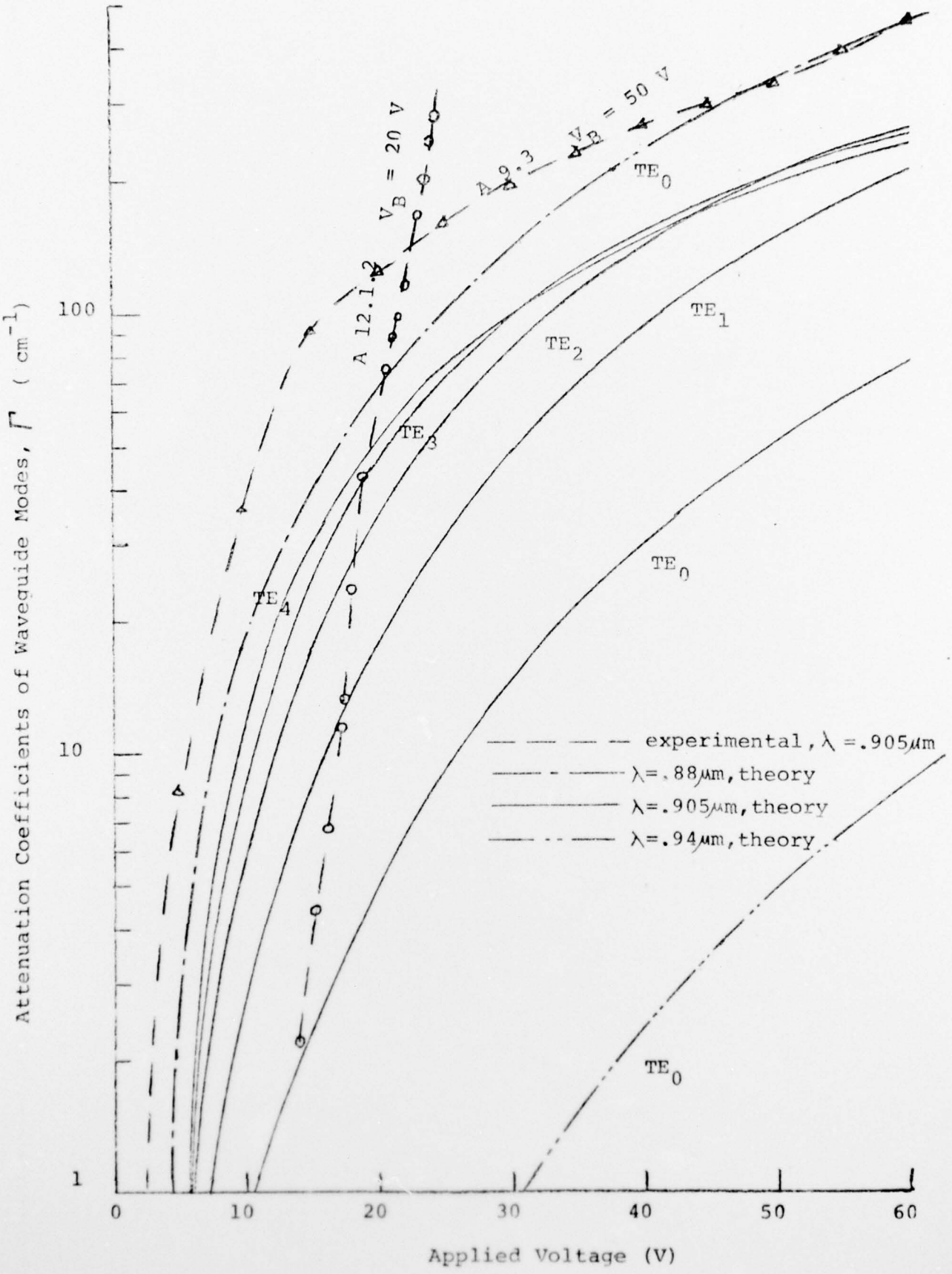

Fig. 3 The Absorption and Attenuation of EAP Waveguide Detectors

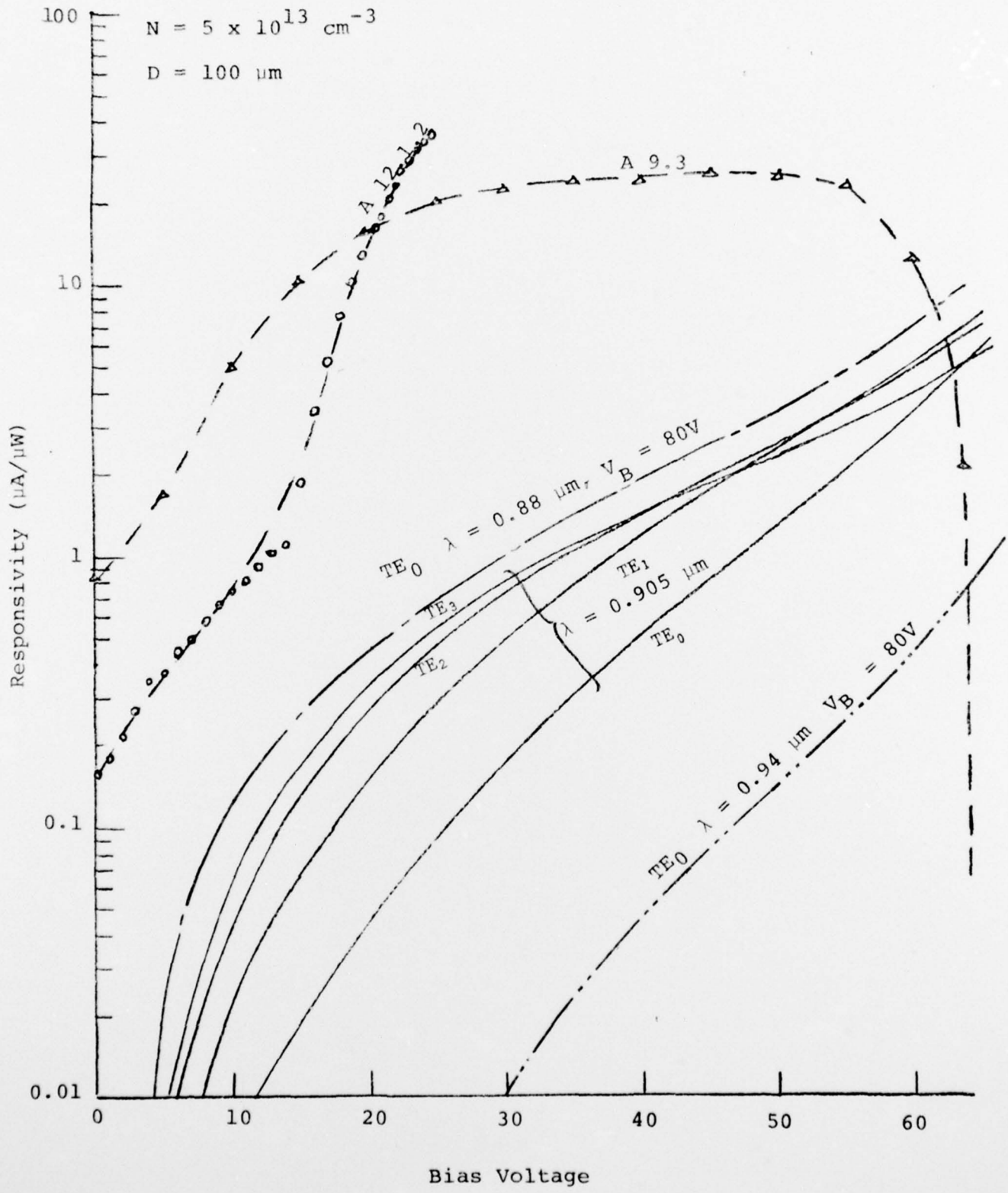

Fig. 4 The Responsivity of the EAP Waveguide Detectors

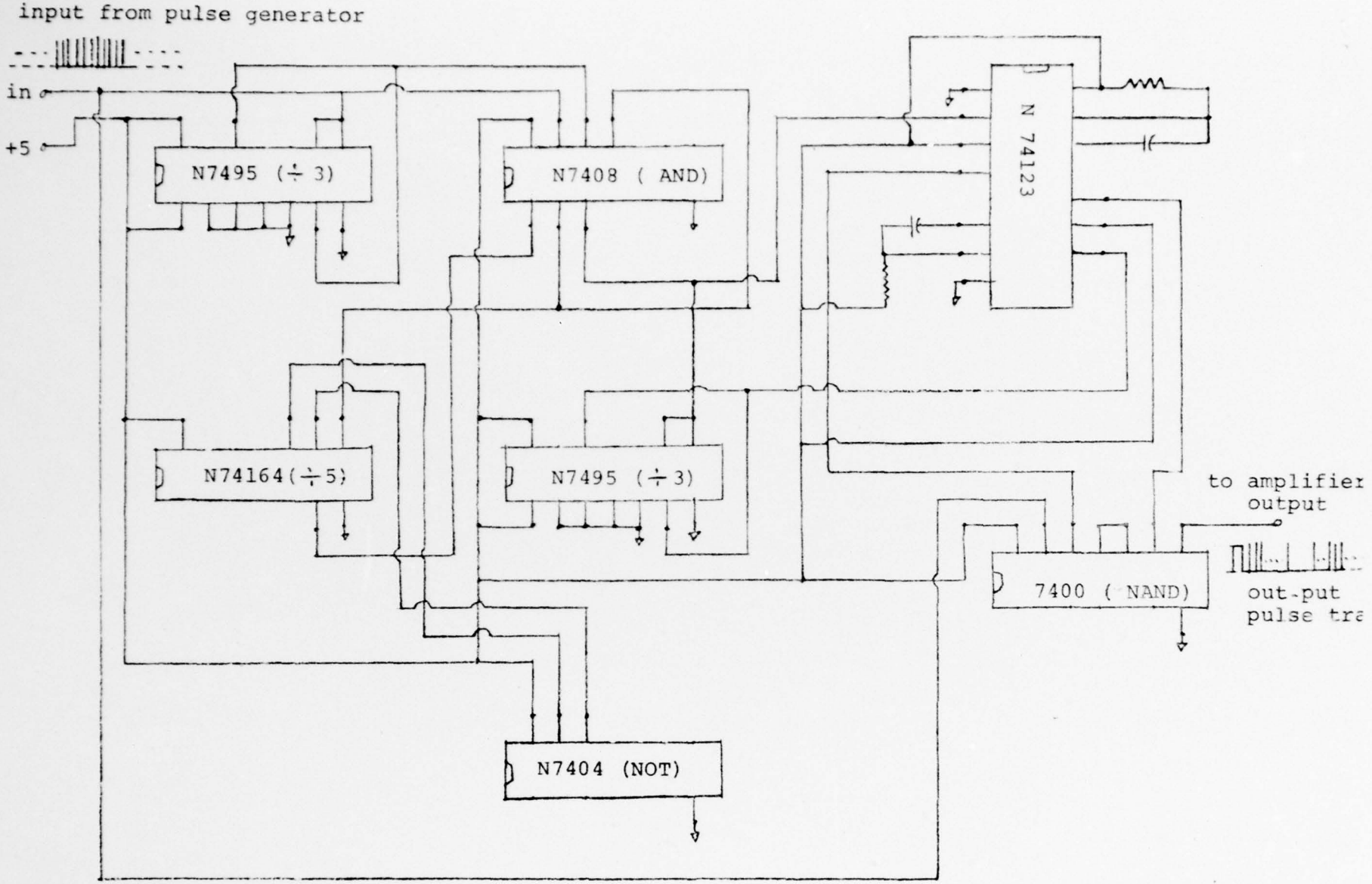

Fig. 5 The Logic Circuits for Generating the Transmitter Pulses

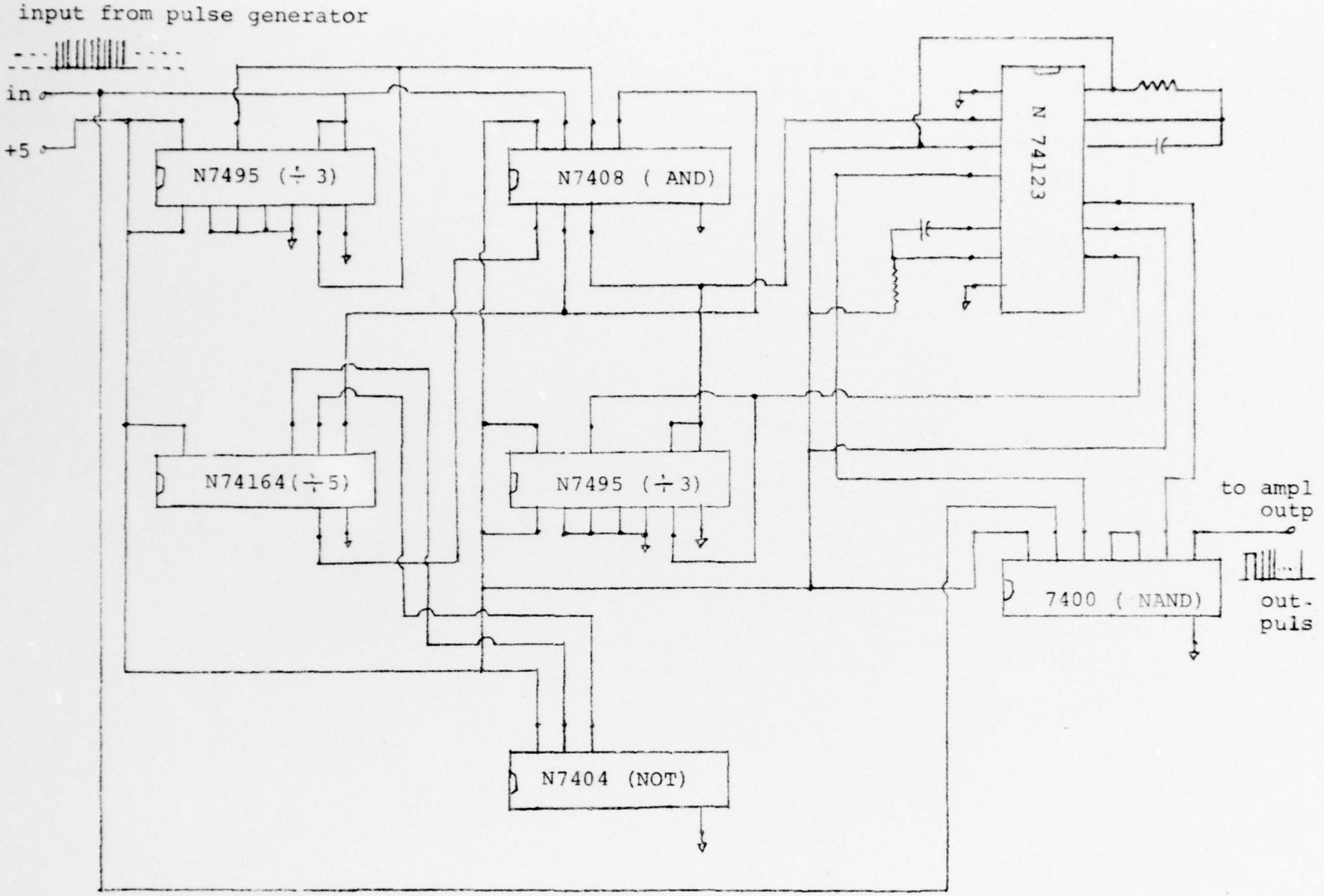

Fig. 5 The Logic Circuits for Generating the Transmitter Pulses

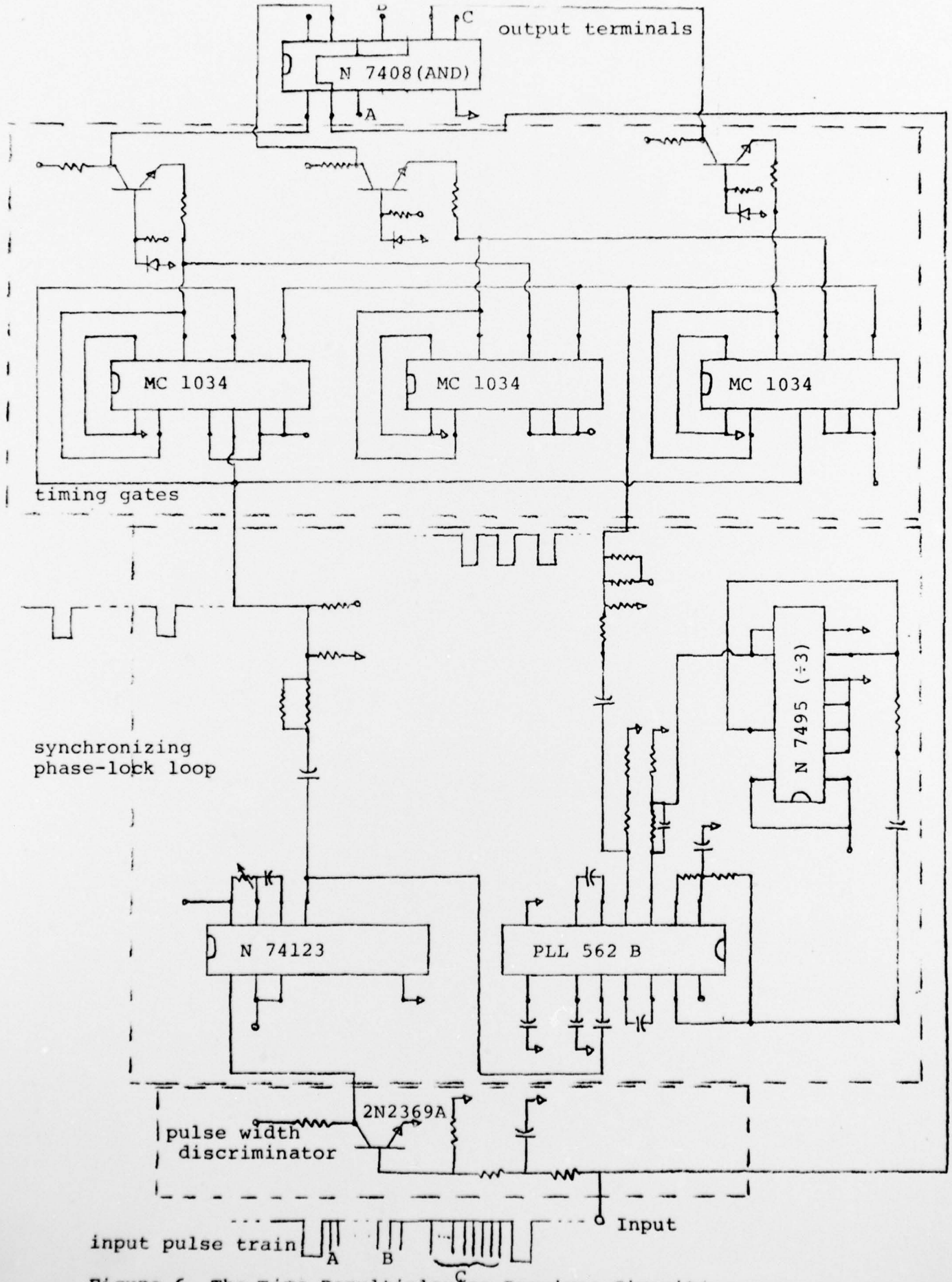

Figure 6 The Time Demultiplexing Receiver Circuits

First Design

$\lambda(\mu m)$		Det.1 s=.1	2 s=.4	3 s=.95
o.88	a	.84	.16	0
	b	.16	0	0
.905	a	.05	.81	.14
	b	.95	.14	0
0.94	a	0	.12	.73
	b	1	.88	.15

Second Design

$\lambda(\mu m)$		Det.1 s=.2	2 s=.4	3 s=.95
0.88	a	1	0	0
	b	0	0	0
.905	a	.32	.59	.09
	b	.68	.09	0
.94	a	.01	.12	.72
	b	.99	.87	.15

s = ratio of applied voltage to the breakdown voltage

a = fraction of the incident power absorbed

b = fraction of the incident power transmitted

D = 100 μm

Table 1 Two Frequency Demultiplexing Schemes